Development and characterization of Fe ultrathin films on the $SrTiO_3$(100) surface

2008 J. Phys.: Condens. Matter 20 315009

(http://iopscience.iop.org/0953-8984/20/31/315009)

J. Phys.: Condens. Matter **20** (2008) 315009 (6pp) doi:10.1088/0953-8984/20/31/315009

Development and characterization of Fe ultrathin films on the $SrTiO_3(100)$ surface

M Kamaratos, D Vlachos[1] and S D Foulias

Department of Physics, University of Ioannina, PO Box 1186, GR 451 10 Ioannina, Hellas

E-mail: dvlachos@cc.uoi.gr

Received 22 April 2008, in final form 10 June 2008
Published 8 July 2008
Online at stacks.iop.org/JPhysCM/20/315009

Abstract

The adsorption of Fe on the $SrTiO_3(100)$ surface at room temperature has been studied in ultrahigh vacuum by means of Auger electron spectroscopy, low energy electron diffraction, electron energy loss spectroscopy, thermal desorption spectroscopy and work function measurements. The results show that iron probably grows in the mode of successive incomplete layers. For coverages $\geqslant$1.5 ML, a short range 1×1 order appears and the deposited Fe overlayer develops in body-centred cubic structure with Fe(100) $\parallel$ $SrTiO_3(100)$ and crystallographic orientation Fe[110] $\parallel$ $SrTiO_3$[100]. The results of the electron spectroscopies do not indicate any iron oxidation at the metal–oxide interface. Instead, an interaction between the Fe adatoms gradually leads to the metallization of the Fe overlayer. Thus, the Fe/$SrTiO_3(100)$ interface seems to be a rather abrupt metal–oxide interface, which presents a good thermal stability for annealing up to ~800 K. In conclusion, this adsorption system looks ideal for free-standing ultrathin Fe films and low-dimensional structures, useful for technological applications.

1. Introduction

The heteroepitaxial growth of thin metal films on metal–oxide substrates has drawn a lot of attention due to its technological applications in many scientific fields such as catalysis (oxide-supported transition metal catalysts), microelectronics and photovoltaic devices (metal–oxide electrical contacts), magnetoelectronic devices (metal–oxide tunnel junctions), functional ceramics with metals, gas sensors, novel materials industry, etc [1–4]. The electrical, mechanical, thermal and chemical properties of these technologically important devices are crucially dependent on the structure, morphology, composition and the stability of the metal–oxide interface [5]. These factors, in turn, are to a great extent determined by (1) the interfacial charge redistribution (electronic interaction) and (2) the interfacial atom transport (chemical interaction) [4]. In fact, there is a strong interplay between these two kinds of interactions. On the one hand, the electronic charge transfer across the interface is influenced by the chemical reactions, while on the other hand the electric fields created by the charge transfer affects the interface reactions or diffusion dynamics [6].

An important question in metal–oxide systems concerns the relation between the metal–oxide interaction at the interface and the growth mode of the metal adsorbate on the substrate. At thermodynamic equilibrium, if the enthalpy of the adsorbate oxide formation is more negative than that of the oxide substrate, the metal reduces the surface forming an intermediate oxide layer between the metal overlayer and the substrate. In addition, in the ultrathin metal film regime (a few atomic layers thickness), diffusion, epitaxial constraints and mixed oxides formation are potentially contributing factors, which also influence the electronic, structural and chemical properties of the metal–oxide interface.

So far, the most used metal–oxide substrates for metal adsorption systems are TiO_2, MgO, ZnO and Al_2O_3 [2], while substrates such as CaO, CeO_2 ZrO_2, WO_2, NiO and CuO are more rarely used. In recent years, however, a lot of investigation has been focusing on the perovskite type oxide surfaces of the form ABO_3, where A is a group II metal and B is a d-metal. One of the most widely studied perovskites is the $SrTiO_3$ (for simplicity henceforth denoted as STO) [7–10]. This oxide is an important substrate for the growth of high-T_c superconducting thin films [11, 12], while it is also used as a high temperature oxygen sensor because of the macroscopic changes of its electrical conductivity [13–15]. In

[1] Author to whom any correspondence should be addressed.

addition, among other oxides, STO has been used as a magnetic barrier in magnetic tunnel junctions [16]. In these junctions, the magnetic barriers between the two magnetic layers are amorphous or crystalline oxide layers. A quite common ferromagnetic metal used in the magnetic tunnel junctions is Fe [17, 18]. In general, it is expected that the various properties of the metal–oxide interface affect the performance of the magnetoelectronic and other nanostructured devices. Therefore, it would be interesting to investigate the Fe/STO interface.

Up to now only a few studies of the development of Fe thin films on $SrTiO_3$ have been done. In particular, Cho *et al* [19, 20] studied the crystal growth of Fe on inclined STO(100) substrates and concluded that Fe films are grown in two parts; one lower part consists of a continuous film and an upper part featuring cluster coagulation. The authors also determined the crystalline orientational relationship between Fe and STO to be Fe(001)[110] ‖ STO(001)[100] and they finally concluded that the morphology of the Fe layers strongly depends on the film thickness. More recently, Silly and Castell [21] investigated the structure and the morphology of self-assembled iron nanocrystals, supported on an $SrTiO_3(001)$-$c(2 \times 4)$ reconstructed surface. They documented an epitaxial growth of Fe in a body-centred cubic structure (bcc) and a truncated pyramidal shape of the nanocrystals. Finally, Ono and Shinjo [22], by growing Fe/Cr(100) multilayers on STO(100) substrates, observed the epitaxial growth of Fe in two phases; one major phase with an in-plane relationship of Fe[110] ‖ STO[100] and a minor one with Fe[111] ‖ STO[100]. The authors attributed these two different phases to the coexistence of TiO_2 and SrO domains on the ordinary strontium titanate substrate.

Despite the above-mentioned works, we believe that the Fe/STO(100) interface has received less attention than it deserves. Therefore, in this work, we investigate the development of ultrathin Fe films on a single $SrTiO_3(100)$ surface at room temperature (RT). Our purpose is to characterize the Fe/STO(100) interface from the electronic, structural and chemical points of view. The development and the characterization start from the submonolayer regime, up to a few monolayers. The study took place in an ultrahigh vacuum (UHV) environment by using Auger electron spectroscopy (AES), electron energy loss spectroscopy (EELS), low energy electron diffraction (LEED), thermal desorption spectroscopy (TDS) and measurements of the relative work function (WF).

2. Experimental details

The experiments were performed in an UHV chamber with a base pressure of the order of 10^{-10} mbar. The chamber was equipped with a four-grid LEED optics, a cylindrical mirror analyser (CMA) with energy resolution 0.3% for the AES and EELS measurements, a quadrupole mass spectrometer (QMS) for gas analysis and the TDS measurements, and an electron gun for the measurements of the relative WF. The chamber was also equipped with an Ar^+ ion sputtering system for sample cleaning and heating facilities. The AES and EELS measurements were recorded in the first derivative mode and the intensity of the Auger and loss lines was measured from the peak-to-peak height (AP-PH).

Iron was evaporated from a well-degassed home-made evaporation source, which consists of a spectrally pure iron filament wrapped around a resistively heated tungsten wire. The evaporation rate was controlled by the current through the W wire. During the Fe deposition, the STO substrate was about 5 cm away from the Fe source to ensure a homogeneous deposition. The source assembly was outgassed many times until no oxygen or carbon contamination was detected on the deposited films. The pressure during the Fe evaporation did not rise to more than 3×10^{-9} mbar, while the sample temperature was close to RT. The atomic flux of the Fe source was calibrated by Auger measurements of the Fe deposition on an Si(100)2×1 surface, which was mounted in the UHV chamber next to the STO sample. According to previous results [23], Fe grows on the Si(100)2×1 surface at RT with a layer-by-layer mode, with the attenuation coefficient (transmission factor) of Si (91 eV) Auger transition line to be $\alpha_{\mathrm{Si,Fe}} = 0.61$ for one layer of Fe. One layer of iron corresponds to an atomic density equal to the density of the Si(100) outermost layer, 6.78×10^{14} at cm^{-2}. According to our calibration process, each Fe dose (1 D) corresponds to $(1.36 \pm 0.05) \times 10^{14}$ at cm^{-2}. 1 D represents the deposited quantity of Fe on STO, when operating the evaporation source at 9.0 A for 30 s.

The STO(100) sample with dimensions $(10 \times 5 \times 1)$ mm^3 was provided by Crystal GmbH. The sample was polished on one side and was doped by Fe acceptors (0.14 wt%). The STO surface was TiO_2-terminated with atomic density 1.97×10^{15} at cm^{-2}. The sample was mounted in a case of tantalum, with a Ta foil strip uniformly pressed between the case and the sample. The STO crystal could be heated by passing current through the Ta foil strip. The temperature was measured by a Cr–Al thermocouple, spot welded onto the back side of the case and calibrated with an infrared pyrometer. The surface was cleaned by heating at 1050 K for several hours. This procedure produces a good 1×1 LEED pattern. However, a small amount of carbon contamination was detected by AES. The carbon contamination was removed by Ar^+ bombardment (2 keV, 1 μA, ∼30 min) and subsequent heating at 900 K. The substrate was considered clean, when the carbon, C (273 eV) to O (510 eV) Auger peak height ratio was less than 5%.

3. Results and discussion

We started to deposit Fe on the STO surface in steps of increasing doses followed by AES measurements. Figure 1 shows the intensity of the Auger lines of Fe (47 eV), Fe (650 eV), O (510 eV), Ti (380 eV) and Sr (110 eV) as a function of Fe doses on the STO(100) surface at RT. Assuming that the sticking coefficient of Fe on STO is the same as that on Si, 1 D of Fe corresponds to the adsorbed density 1.36×10^{14} at cm^{-2}. In this work we define one monolayer (ML) of Fe to be equal to the atomic density of the $TiO_2(100)$ surface. Therefore a relation between doses and coverage in MLs can be found as it is shown on the top x axis in figure 1. We note that one physical layer of Fe is smaller than 1 ML as defined here. The AP-PHs of the Fe Auger

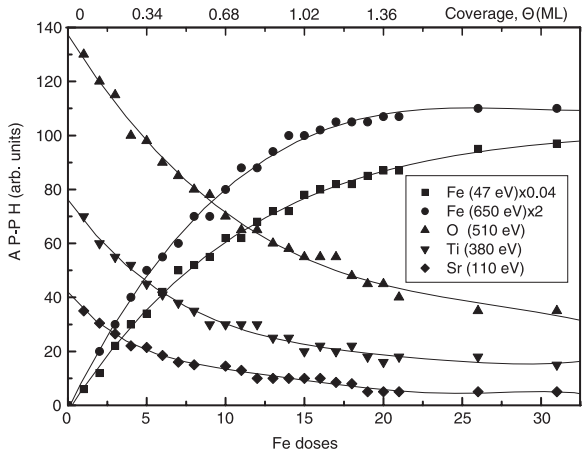

Figure 1. The AP-PHs of Fe (47 eV), Fe (650 eV), O (510 eV), Ti (380 eV) and Sr (110 eV) Auger lines versus Fe doses on the STO(100) surface at RT. The estimated coverage in ML is also shown. Polynomial lines are drawn as guides to the eye.

transition lines increase, while those of the substrate ones decrease analogously. Since the scattering of the data does not allow us to identify any unambiguous breaks (although we cannot rule out their presence and thus a piecewise linear curve), polynomial lines have been drawn to guide the eye. This nonlinear Auger signal variation may be due to either the formation of three-dimensional clusters (VW mode) or to the evolution of successive incomplete layers [24]. The latter growth mode, which is known as simultaneous multilayers (SM mode), is more likely since the attenuations of the substrate signals are too large to be explained by the VW mechanism. Indeed, for 7 D of Fe, which is approximately one physical layer of Fe, the attenuation coefficient of the O (510 eV) Auger signal is 0.63, that of the Ti (380 eV) 0.50 and that of the Sr (110 eV) 0.41. Taking into account the respective inelastic mean free paths of the Auger electrons [25], these attenuations are not compatible with the VW mode. Another indication supporting the SM growth could be the appearance of a diffuse (1 × 1) LEED pattern at higher Fe coverages, as we discuss later. We note that the SM growth mode has been observed for Ni ultrathin film development on the STO(100) surface [26]. However, Cho *et al* [19] using scanning tunnelling microscopy concluded that the morphology of Fe overlayers on the inclined STO(100) surface depends on the film thickness. In particular, the authors concluded that Fe initially forms isolated clusters, which gradually coalesce as the coverage increases, to form a continuous layer with the upper part to be in the shape of coagulation clusters. Although a direct comparison between the inclined and our rather flat STO surface is not quite appropriate, we cannot exclude that in our case the successive incomplete layers of iron might coalesce gradually to a uniform layer with the top of the layer resembling large clusters.

We also performed LEED measurements, which showed that the deposition of Fe on the STO(100) surface caused the gradual disappearance of the 1 × 1 substrate symmetry in rather early adsorption stages. However, for coverages $\geqslant$1.5 ML, a new strongly diffuse (1 × 1) LEED pattern appeared. The LEED pattern configurations of the clean and the Fe (2.5 ML)/STO(100) surface are shown in figures 2(a) and (b), respectively. The spots of the Fe (1.5 ML)/STO(100) diffraction pattern were initially very broad but progressively

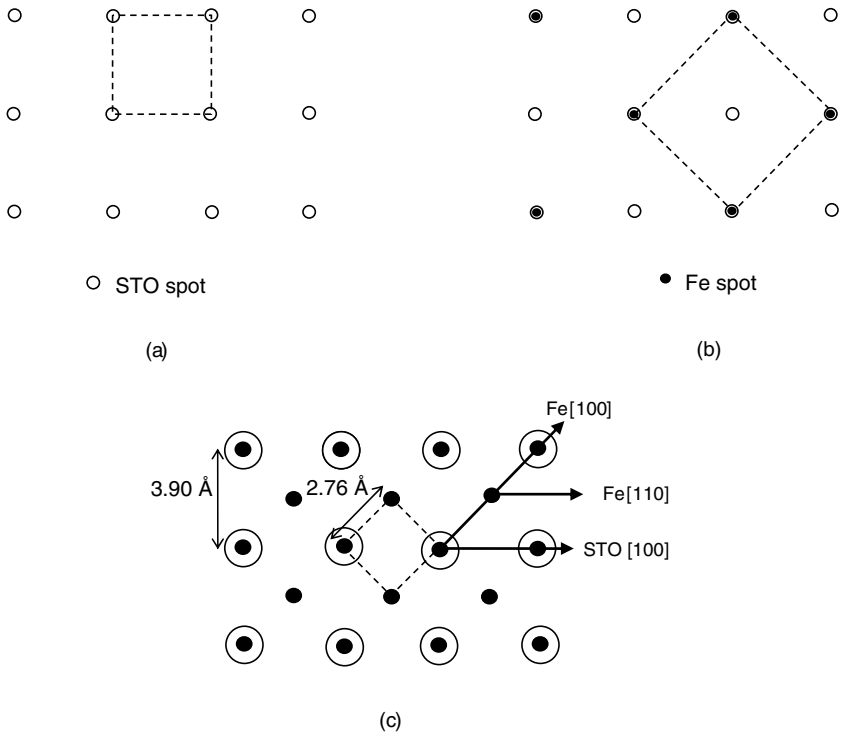

Figure 2. LEED pattern configuration of (a) the clean STO(100) surface and (b) the Fe (2.5 ML)/STO(100) surface. (c) A model of the direct atomic lattice of Fe on STO(100) is shown, with the full and the open cycles representing the Fe and the Ti surface atoms, respectively. The dashed square shows the surface lattice unit shell.

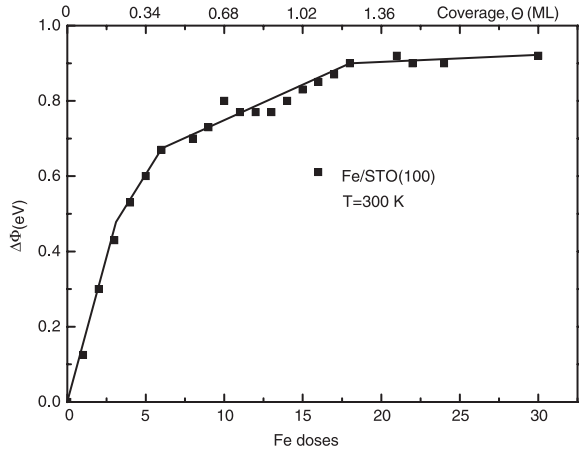

Figure 3. The WF change, $\Delta\Phi$, of the STO(100) surface as a function of Fe doses and coverage at RT.

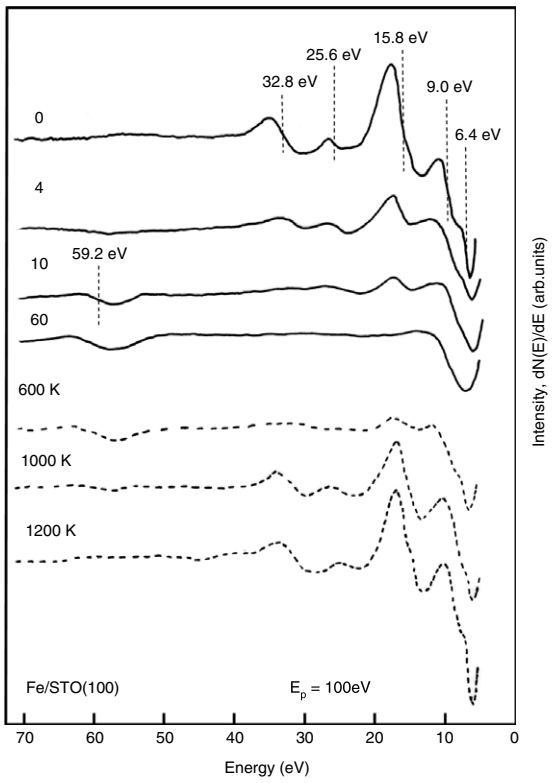

Figure 4. The EELS measurements of the STO(100) surface covered with different amounts of Fe at RT (solid lines) and after annealing at several temperatures (dashed lines). The electron primary energy is $E_p = 100$ eV.

they became sharper as the coverage was increased. At a coverage of about 2.5 ML, however, the diffraction spots were much broader than those of the clean STO(100) surface. This indicates a poor long range ordering of the Fe overlayer. The adatom–adatom distance was estimated by a routine LEED pattern analysis and found to be 0.276 nm. This value is close to 0.287 nm [27], the distance between the atoms in the Fe(100) plane of the bcc structure. This finding suggests that, at least for coverages of a few MLs, Fe grows in a bcc structure with the Fe(100) ‖ STO(100) and Fe[110] ‖ STO[100] as figure 2(c) demonstrates. The same epitaxial orientation relationship has been found for Mo and Cr thin film development on the STO(100) surface by Wagner *et al* [28], who proposed that the adsorbate epitaxial growth depends on the oxygen affinity of the metal P_O and the lattice mismatch f of the metal with the substrate. According to the authors' results, a diagram showing the relation between epitaxy, P_O and f is presented. In this diagram, Fe is predicted to show epitaxy in accordance with our results. The same orientation was also found by other investigators [19, 20, 22], while a bcc(100) epitaxy has been observed for Fe overlayers on TiO_2(110) [29].

Figure 3 shows the change of the WF, $\Delta\Phi$, of the STO(100) surface as a function of the Fe doses and coverage at RT. $\Delta\Phi$ seems to increase piecewise linearly before the completion of the first ML. Finally, $\Delta\Phi$ levels off at higher coverages (>1.1 ML). Considering our previous photoemission measurements at the cutoff [30], the WF of our clean STO(100) surface is about 3.4 eV. Thus, the WF of the Fe (>1.1 ML)/STO(100) surface should be ∼4.3 eV. This value is close to the work function of the Fe(100) surface (4.67 eV) [31], which is an indication that, during the formation of the second ML, the adsorbate should approach the metallic phase.

Figure 4 shows the EELS measurements of the STO(100) surface with different Fe doses. The energy of the incident electron beam was 100 eV and the EELS curves were recorded in the $dN(E)/dE$ mode. The loss spectrum of the clean STO surface shows lines at about 6.4, 9.0, 15.8, 25.6 and 32.8 eV, and looks quite similar to the previously recorded curve by Andersen and Møller [32]. The low energy losses at 6.4 and 9.0 eV are assigned to interband valence band transitions between occupied O 2p bands and unoccupied Ti 3d states [33], while the 15.8 eV loss line might be attributed to a transition from the Sr 4p to the Ti 3d empty states [34]. The higher energy loss line at ∼25.6 eV may be due to a bulk plasmon loss since such a plasmon has been previously reported at 26.4 eV [33, 35]. Finally, the 32.8 eV line, according to previous studies, can be interpreted as transitions from the states Sr 4p, O 2s, Ti 3p or Sr 4s to final states in the conduction band or to localized excited states [35, 36]. As iron starts to grow on STO, all the substrate loss lines begin to decline. At about 10 D, a new line at ∼59 eV appears, which progressively becomes stronger as the coverage increases. This loss is attributed to an excitation from the Fe 3p levels. The Fe bulk plasmon loss line at ∼22 eV is hardly observed. A weak plasmon peak has also been measured during Fe deposition on the Si(100) surface [23]. After the annealing above 950 K, the low energy loss lines of the substrate reappear, whereas the Fe 3p line almost disappears. This probably indicates that the adsorbate desorbs from the surface under such conditions. Indeed, this was confirmed by independent TDS measurements (see below), where desorbing Fe atoms were detected for substrate annealing higher than 800 K. For annealing temperature ∼1200 K, the clean STO loss spectrum clearly reappears.

From the chemical point of view, an important issue is whether any chemical interaction takes place at the interface

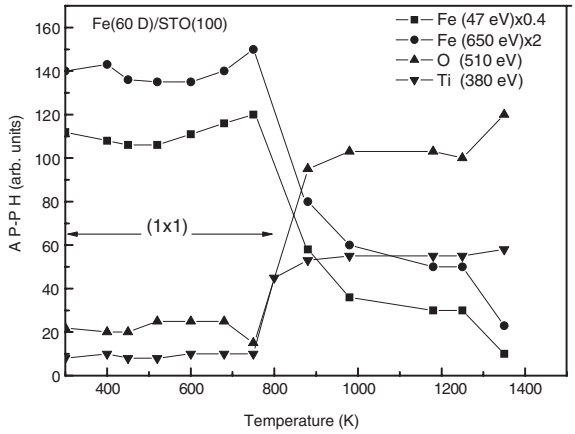

Figure 5. The AP-PHs of Fe (47 eV), Fe (650 eV), O (510 eV) and Ti (380 eV) Auger transition lines as a function of the substrate temperature for 20 s anneals. The annealed surface is the Fe (60 D)/STO(100). Note that the 1 × 1 symmetry remains for annealing up to about 800 K.

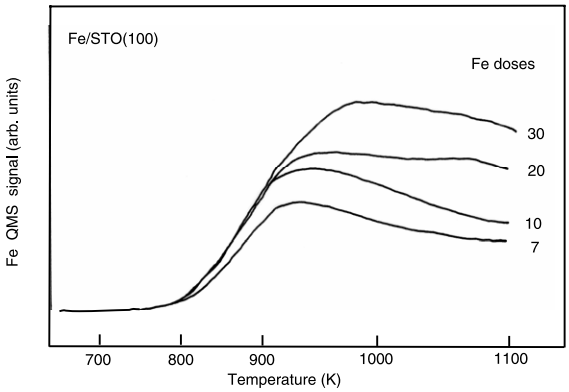

Figure 6. TDS measurements of Fe (56 amu) for Fe deposition on the STO(100) surface. The disproportion in the temperature axis is due to the flash desorption mode where the desorption spectra have been recorded.

between the Fe and the top O atoms. Such an interaction will result in the oxidation of the adsorbate with the reduction of the STO at the same time. Numerous previous studies on the iron oxidation on surfaces [37–42] have shown that the low energy AES spectrum around the Fe($M_{23}M_{45}M_{45}$) Auger transition line of the metallic Fe drastically changes as the iron oxide is developing. In fact, this Auger transition is a core valence–valence intraband transition involving the valence band density of states. It is therefore expected that the lineshape and the energy of this Auger line will be strongly affected by the chemical environment of the Fe adatoms. In the case of the formation of iron oxides such as Fe_2O_3 or Fe_3O_4, the disappearance of the metallic Fe Auger line is expected along with the simultaneous appearance of two new lines at about 43 and 52 eV, respectively [37, 40–42]. Although we recorded in detail the energy range around the Fe ($M_{23}M_{45}M_{45}$) Auger transition line at about 47 eV, no new lines were recorded. This probably means that oxidation of Fe does not take place at the interface. Further, the EELS measurements (figure 4) do not indicate any oxidation of the adsorbate, because Fe deposition did not induce any new loss lines in the low energy range (<10 eV). In contrast, Sakisaka *et al* [43], oxidizing a Fe(100) surface and forming bulk γ-Fe_2O_3, recorded loss peaks at ∼3.6 and 6.6 eV ascribed to the $O^{2-}(2p) \rightarrow Fe^{3+}(3d)$ charge transfer transition.

Figure 5 demonstrates the AP-PHs of Fe (47 eV), Fe (650 eV), O (510 eV) and Ti (380 eV) Auger transition lines as a function of the temperature after the deposition of 60 D (∼4 ML) of Fe on the STO(100) surface. The intensities of the Fe Auger lines initially decrease up to ∼450 K and then increase up to ∼750 K. Above 800 K the AP-PHs of the Fe lines decrease rapidly up to about 1000 K and remain almost constant for up to ∼1250 K. Finally, the intensities decrease again at even higher temperatures. The AP-PHs of the substrate Auger lines increase analogously whenever the Fe signals decrease. A small amount of Fe (∼0.15 ML) always remains on the surface even after strong annealing at 1350 K. This adsorbate quantity is removable only by Ar^+ ion sputtering.

The small increase of the Fe signal intensity just before 800 K is accompanied by a small improvement of the (1 × 1) LEED pattern, with sharper diffraction spots. This might be attributed to a rearrangement of the Fe adatoms on the surface enhancing the bcc symmetry of the substrate and showing that the Fe (1 × 1)/STO(100) interface remains quite stable even after annealing up to about 800 K. The decrease of the Fe Auger signals, when the substrate temperature exceeds 800 K, is explained by Fe desorption from the surface. This was verified by independent TDS measurements, which are presented in figure 6. The thermal desorption spectra were taken in the flash desorption mode, which explains the nonlinear temperature axis. As the QMS signal shows, Fe desorbs in elemental form. Despite tuning to all relevant atomic mass units, no iron oxide compound such as Fe_2O_3 or FeO was ever detected. This is additional evidence that no oxidation process occurs at the Fe/STO interface.

4. Summary

In this work we developed and characterized Fe thin films on the $SrTiO_3$(100) surface at room temperature. The investigation was carried out by LEED, AES, EELS, TDS and WF measurements. The results show that Fe grows probably in the form of successive incomplete layers presenting a short range 1 × 1 symmetry at coverages higher than 1.5 ML. The development of the iron overlayer occurs in body-centred cubic structure with Fe(100) ‖ $SrTiO_3$(100) and crystallographic orientation Fe[110] ‖ $SrTiO_3$[100]. It seems that no chemical interaction between the Fe adatoms and the top surface O atoms takes place, establishing a rather sharp and stable metal–oxide interface. The thermal stability of the system up to about 800 K may be important for technological applications.

References

[1] Campell C T 1997 *Surf. Sci. Rep.* **27** 1
[2] Henry C R 1998 *Surf. Sci. Rep.* **31** 235
[3] Finnis M W 1996 *J. Phys.: Condens. Matter* **8** 5811
[4] Fu Q and Wagner T 2007 *Surf. Sci. Rep.* **62** 431

[5] Ernst F 1995 *Mater. Sci. Eng.* R **14** 97
[6] Brillson L J 1982 *Surf. Sci. Rep.* **2** 123
[7] Hill D M, Meyer H M III and Weaver J H 1989 *J. Appl. Phys.* **65** 4943
[8] Wagner T, Richter G and Rühle M 2001 *J. Appl. Phys.* **89** 2606
[9] Fu Q and Wagner T 2002 *Surf. Sci.* **505** 39
[10] van Benthem K, Scheu C, Sigle W and Rühle M 2002 *Z. Metallk.* **93** 362
[11] Chaudhari P, Koch R H, Laibowitz R B, McGuire T R and Gambino R J 1987 *Phys. Rev. Lett.* **58** 2684
[12] Jiang Q D, Smilgies D M, Feidenhans R, Cardona M and Zegenhagen J 1996 *Solid State Commun.* **98** 157
[13] Menesklou W, Schreiner H J, Härdtl K H and Ivers-Tiffée E 1999 *Sensors Actuators* B **59** 184
[14] Zhou X, Sorensen O T, Cao Q and Xu Y 2000 *Sensors Actuators* B **65** 52
[15] Wagner S F, Warnke C, Menesklou W, Argirusis C, Damjanović T, Borchardt G and Ivers-Tiffée E 2006 *Solid State Ion.* **177** 1607
[16] De Teresa J M, Barthélémy A, Fert A, Contour J P, Montaigne F and Seneor P 1999 *Science* **286** 507
[17] Smith D J, McCartney M R, Platt C L and Berkowitz A E 1998 *J. Appl. Phys.* **83** 5154
[18] Faure-Vincent J, Tiusan C, Jouguelet E, Canet F, Sajieddine M, Bellouard C, Popova E, Hehn M, Montaigne F and Schuhl A 2003 *Appl. Phys. Lett.* **82** 4507
[19] Cho G B, Yamamoto M and Endo Y 2004 *Sci. Technol. Adv. Mater.* **5** 89
[20] Cho G B, Yamamoto M and Kamada Y 2002 *Japan. J. Appl. Phys.* **41** 5713
[21] Silly F and Castell M R 2005 *Appl. Phys. Lett.* **87** 063106
[22] Ono T and Shinjo T 1999 *Surf. Sci.* **438** 341
[23] Gallego J M and Miranda R 1991 *J. Appl. Phys.* **69** 1377
[24] Argile C and Rhead G E 1989 *Surf. Sci. Rep.* **10** 277
[25] Tanuma S, Powell C J and Penn D R 1991 *Surf. Interface Anal.* **17** 911
[26] Vlachos D, Kamaratos M, Foulias S D, Argirousis C and Borchardt G 2004 *Surf. Sci.* **550** 213
[27] Kittel C 1986 *Introduction to the Solid State Physics* 6th edn (New York: Wiley)
[28] Wagner T, Polli A D, Richter G and Stanzick H 2001 *Z. Metall.* **92** 7 references therein
[29] Mei Pan J, Maschhoff B L, Diebold U and Madey T 1993 *Surf. Sci.* **291** 381
[30] Kamaratos M, Vlachos D and Foulias S D 2004 *Surf. Rev. Lett.* **11** 419
[31] Ueda K and Shimizu R 1972 *Japan. J. Appl. Phys.* **11** 916
[32] Andersen J E T and Møller P J 1990 *Thin Solid Films* **186** 137
[33] Henrich V E, Dresselhaus G and Zeiger H J 1979 *Phys. Rev.* B **17** 4908
[34] van Benthem K, French R H, Sigle W, Elsässer C and Rühle M 2001 *Ultramicroscopy* **86** 303
[35] Kohiki S, Oku M and Waseda Y 2000 *Phys. Rev.* B **62** 7964
[36] Bermudez V M and Ritz V H 1980 *Chem. Phys. Lett.* **73** 160
[37] Seo M, Lumsden J B and Staehle R W 1975 *Surf. Sci.* **50** 541
[38] Miyano T, Sakisaka Y, Komeda T and Onchi M 1986 *Surf. Sci.* **169** 197
[39] Smentkowski V S and Yates J T Jr 1990 *Surf. Sci.* **232** 113
[40] den Daas H, Gijzeman O L J and Geus J W 1993 *Surf. Sci.* **290** 26
[41] Sault A G 1994 *Appl. Surf. Sci.* **74** 249
[42] Qin F, Magtoto N P, Garza M and Kelber J A 2003 *Thin Solid Films* **444** 179
[43] Sakisaka Y, Miyano T and Onchi M 1984 *Phys. Rev.* B **30** 6849